Kashf Journal of Multidisciplinary Research
Vol:03 - Issue02(2026)
P-ISSN: 3007-1992 E-ISSN: 3007-200X
https://kjmr.com.pk

FINITE ELEMENT ANALYSIS OF INCOMPRESSIBLE FLUID FLOWS IN A BACKWARD STEP DUCT USING COMSOL MULTIPHYSICS

Murtaza Hussain Shar[1], Akhalque Ahmed Abbasi[2], Mazhar Ali Sahito[3], Rabia Parveen Memon[4] *Dr. Abdul Raheem Shar[5], Muzamil Hussain Shar[6]

[1, 5]Asistant Professor Govt. Degree College Thari Mirwah, Pakistan.

[2, 3]Lecturer, GRA, Govt Degree College Kandiaro, Pakistan.

[4, 6]Shah Abdul Latif University Khairpur, Sindh, Pakistan.

Corresponding Author:(araheem.shar@salu.edu.pk)

DOI:(*https://doi.org/10.71146/kjmr850*)

Article Info

Abstract

This study presents a numerical investigation of Newtonian fluid flow through a backward step duct using the Galer kin Least Square Finite Element Method (GLSFEM) within the COMSOL Multiphysics environment. The research explores the impact of fluid inertia and geometric variations on flow characteristics, specifically focusing on aspect ratios of 1:6 and 1:12. By solving the incompressible stationary and non-stationary Navier-Stokes equations, the simulation characterizes vortex formation, recirculation flow rates, and reattachment lengths across a range of Reynolds numbers. Results indicate that increasing the Reynolds number and expansion ratio significantly enhances the intensity and length of primary and secondary eddies at the duct corners. Quantitative analysis is supported by newly developed empirical equations for recirculation flow rates, which demonstrate high correlation with existing literature. The findings provide critical insights for industrial applications involving flow separation and mixing, such as automotive silencers, chemical transport tanks, and turbine blade design.

Keywords:
Computational Fluid Dynamics (CFD), Galer kin Least Square Finite Element Method, Backward Step Duct, Newtonian Fluid, Recirculation Flow, Vortex Phenomena.

INTRODUCTION

Computational Fluid Dynamics (CFD) serves as a bridge between pure theory and physical experimentation [1]. It involves the use of numerical analysis and data structures to analyze and solve problems that involve fluid flows. In modern engineering, CFD is indispensable for predicting how fluids interact with surfaces and internal geometries. By discretizing the continuous domain into a finite number of elements, complex partial differential equations (PDEs)—which are often impossible to solve analytically—can be approximated with high precision [2,3]

The study of fluid flow in a backward step duct is governed by the incompressible Navier-Stokes equations, which represent the fundamental principles of the conservation of mass and the conservation of momentum. For an incompressible Newtonian fluid, mass conservation is expressed by the continuity equation$\nabla \cdot \mathbf{u}=0$ [4,5]. While the conservation of momentum is defined as, $\rho(\frac{\partial u}{\partial t} + u \cdot \nabla u) = -\nabla p + \mu \nabla 2u + f$,in these expressions, $\frac{\partial \boldsymbol{u}}{\partial t}$represents the velocity vector, p denotes the pressure, ρ is the fluid density, and μ refers to the dynamic viscosity [6,7]. In the context of this topic, either stationary or steady-state conditions and non-stationary or transient conditions are analyzed to provide a comprehensive understanding of how flow patterns either evolve over time or stabilize under constant boundary conditions [8].

The "backward step" or "sudden expansion" duct is classic benchmark geometry in fluid mechanics, consisting of a narrow inlet channel that abruptly opens into a wider expansion area [9].This geometry is scientifically significant because it triggers several critical fluid phenomena, beginning with flow separation, where the fluid can no longer remain attached to the wall as it passes the sharp corner of the step.This separation results in the creation of a low-pressure zone behind the step, leading to recirculation and the formation of eddies, specifically a primary vortex known as the recirculation zone. At higher Reynolds numbers, this phenomenon becomes more complex as secondary vortices may appear at the upper corners or further downstream. Eventually, the separated flow reaches a point where it reattaches to the bottom wall, and the distance from the step to this specific location is defined as the reattachment length, which serves as a key quantitative metric in this study [10].To solve the governing equations within the backward step geometry, this research employs the Galer kin Least Square Finite Element Method (GLSFEM) [11]. Traditional Galer kin methods often suffer from numerical instabilities (oscillations) when dealing with convection-dominated flows (high Reynolds numbers) or when using equal-order interpolation for velocity and pressure [12].GLSFEM overcomes these issues by adding a "least squares" stabilization term to the standard Galer kin formulation. This enhances the stability of the solution without sacrificing accuracy, allowing for a robust calculation of velocity streamlines and pressure gradients even in regions of high turbulence or rapid geometric transition [13].

The simulation is implemented using COMSOL Multiphysics, which is a powerful finite element analysis software. COMSOL allows for a "Multiphysics" approach, meaning it can couple fluid flow with heat transfer or chemical reactions if needed [14,15]. For this specific work, the COMSOL CFD module is utilized to generate high-quality meshes and discretization around the sharp corner of the step where gradients are steepest. It is also used to apply boundary conditions such as “No Slip” at the walls and specific velocity profiles at the inlet, while executing parametric sweeps to compare different expansion ratios of 1:6 versus 1:12 across varying Reynolds numbers [16]. The engineering and industrial significance of this study is substantial, as the study of backward step ducts is not merely

academic but mimics real-world scenarios found in numerous industrial applications. In the automotive industry, it is essential for designing silencers and mufflers for heavy sports vehicles where gas expansion and noise reduction are critical [17]. In the field of aerospace, it aids in understanding flow over air foils and turbine blades where sudden changes in geometry can lead to stall or loss of efficiency. Chemical engineering benefits from this research through the design of mixing tanks and transport routes where "dead zones" or recirculation areas can affect the sedimentation of chemicals or the efficiency of a reaction. Additionally, environmental engineering utilizes these models to understand sedimentation patterns in reservoirs and water treatment facilities [18]. The primary goal of this work is to set the stage for a comparative analysis. By varying the aspect ratio of the duct and the inertia of the fluid (represented by the Reynolds number), this research aims to quantify exactly how the vortex intensity and reattachment length changes? Through the development of new empirical equations, the thesis seeks to provide a predictive tool that can be used by engineers to optimize duct designs for better flow control and energy efficiency

METHODOLOGY

Computational Fluid Dynamics (CFD) has emerged as a vast and essential field by integrating complex mathematical models—specifically partial differential equations—with physical principles and high-performance computing to resolve large-scale problems. This discipline spans across numerous sectors, including medical sciences, aerodynamics, hydraulic engineering, and the automotive industry. Modern CFD relies on sophisticated software packages such as ANSYS, COMSOL Multiphysics, and FlexPDE to design, discretize, solve, and visualize fluid interactions within both open and closed geometries that mirror real-world scenarios. A critical aspect of this process is selecting an appropriate numerical technique to manage the steady-state and transient characteristics of fluid motion, as each method possesses unique limitations despite potential advantages in convergence speed. Given its robust capabilities and widespread industrial relevance, the Finite Element Method (FEM) was utilized in this study via COMSOL Multiphysics, following the established frameworks as given in references of 19, 20 & 21[19-21]. The COMSOL Multiphysics package utilizes the Finite Element Method (FEM) as its core mathematical foundation, offering a broad range of applications through advanced computational algorithms that ensure results meet a specified level of numerical accuracy.

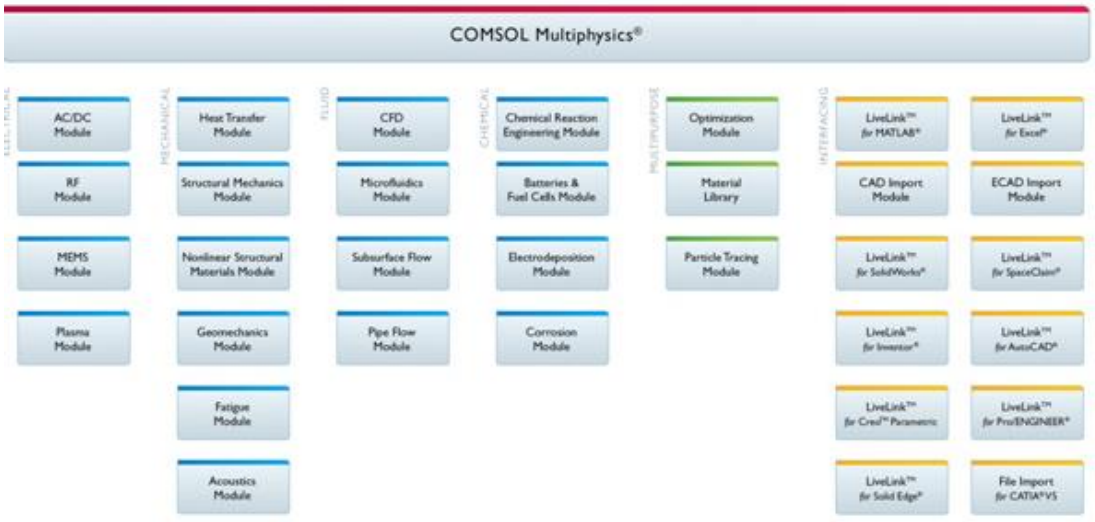

Figure –1: Flow diagram of the COMSOL Multi-Physics

The program includes a large flow chart where a laminar flow issue is selected, followed by the discretization of the governing equations of fluid dynamics using a variety of finite element methods, including Galer kin and Petrov-Galerkin, among others. First, it was explained how the governing equations connect to the project's research topic.

THEORY OF GOVERNING EQUATIONS

The governing theoretical framework is centered on the fundamental conservation laws of physics, specifically the conservation of mass and momentum. Given that the domain consists of a rectangular channel, these principles are expressed here through the continuity and momentum transport equations in two-dimensional Cartesian coordinates. To effectively couple the velocity field and pressure, the equations are defined under the assumptions of Newtonian and incompressible fluid behavior

EQUATIONOF CONTINUITY

The continuity assumption that the fluid transport rate at the body's entrance must match the fluid outflow rate at the body's outlet is the basis for this equation. Due to the scope of interest, this assumption is only formally addressed here in two dimensions and for incompressible fluids;
For Incompressible fluids

$$\frac{\partial u^*}{\partial x^*} + \frac{\partial v^*}{\partial y^*} = 0 \qquad (1)$$

The vector velocity field, denoted as the divergence free vector, is shown here by u and v.

EQUATIONFOR MOMENTUM TRANSPORT

The governing equations employed here describe the transfer of momentum resulting from the coupling of external forces, such as pressure gradients. Derived from Newton's second law of motion—perhaps the most fundamental principle in mechanics—this formulation dictates that the net force acting on a fluid element is directly proportional to its acceleration. The resulting momentum equations are expressed as follows:

$$F = m\,a \qquad (2)$$

In this context, F represents the external force, m is the constant of proportionality (mass), and 'a' denotes the body's acceleration. By incorporating specific fluid properties—including density, dynamic viscosity, the velocity vector field, and pressure—Equation (3.2) can be expanded into its differential form. The general dimensional representation of the momentum transfer equations is provided below:

$$\rho(\mathbf{u}.\nabla)\mathbf{u} = \nabla\left[-pI + \mu\left(\nabla\boldsymbol{u} + (\nabla\boldsymbol{u})^T\right)\right] + F \qquad (3)$$

While Equation (3.3) can accommodate a diverse range of fluid types and flow regimes, this research focuses specifically on the two-dimensional, laminar flow of Newtonian liquids. To streamline the computational process and ensure rapid convergence, the governing equations are presented in their non-dimensional form. By non-dimensional zing the variables, physical properties such as density and viscosity are consolidated into the Reynolds number (Re). This dimensionless parameter represents the ratio of inertial forces to viscous forces, effectively

characterizing the fluid's resistance to flow. The resulting non-dimensional equations for this specific study are as follows:

$$\frac{\partial u^*}{\partial t}+\left(u^*\frac{\partial u^*}{\partial x^*}+v^*\frac{\partial u^*}{\partial y^*}\right)=-\frac{\partial P^*}{\partial x^*}+\frac{1}{\mathrm{Re}}\left[\frac{\partial}{\partial x^*}\left(\frac{\partial u^*}{\partial x^*}\right)+\frac{\partial}{\partial y^*}\left(\frac{\partial u^*}{\partial y^*}\right)\right] \quad (4a)$$

$$\frac{\partial v^*}{\partial t}+\left(u^*\frac{\partial v^*}{\partial x^*}+v^*\frac{\partial v^*}{\partial y^*}\right)=-\frac{\partial P^*}{\partial y^*}+\frac{1}{\mathrm{Re}}\left[\frac{\partial}{\partial x^*}\left(\frac{\partial v^*}{\partial x^*}\right)+\frac{\partial}{\partial y^*}\left(\frac{\partial v^*}{\partial y^*}\right)\right] \quad (4b)$$

Here, Reynolds number, or Re, is referred to as fluid flow inertia and is concentrated as follows:

$$\mathrm{Re}=\frac{\rho\times u_{avg}\times L}{\mu}$$

In contrast, L denotes the channel's length, μ mean denotes the average velocity, and ρ denotes the fluid's density and↑its viscosity.

INITIAL AND BOUNDARY CONDITIONS

The computational domain is composed of three primary sections: two small rectangles representing the inlet and outlet, and a larger central rectangle acting as the tank. Within this geometry, several boundary conditions are established. All external boundaries are defined as stationary walls, requiring the application of the no-slip condition. The right-hand boundary is designated as the outlet with a fixed zero-pressure condition, while the left-hand boundary serves as the inlet under a specified maximum pressure. To visualize the flow patterns within the domain, a parabolic velocity profile is implemented at the inlet, defined by the following expression:

$$u(y)=6\times U_m\times\frac{y}{L}\left(1-\frac{y}{L}\right),\ P\ =\ Pmax \quad (5)$$

NUMERICAL TECHNIQUES THROUGH CFD PACKAGE COMSOL MULTIPHYISCS

Within the framework of partial differential equations (PDEs), the field of CFD provides a mathematical representation of physical laws governing both spatial and transient phenomena. While analytical solutions are generally limited to fundamental problems with simple geometries, complex domains and non-linear PDEs necessitate approximate numerical solutions. In this study, the Finite Element Method (FEM) is employed for the discretization of these governing equations. This discretization process utilizes a structured mesh to transform continuous differential operators into a system of discrete variables across space and time. Once discretized, a stable numerical solver can be applied to calculate the unknown parameters of the PDE. Specifically, the discretization strategy implemented here is the Galer kin method, supplemented by the integration of least-squares residuals to stabilize the shape functions. This computational approach is executed using the COMSOL Multiphysics package.

FINITE ELEMENT METHOD

Historically, this technique was pioneered by the German-American mathematician Richard Courant in the early 1940s. While initially developed to resolve complex problems in structural mechanics—a field where it remains a standard—the method has since expanded into solid and fluid mechanics. Beyond mechanical engineering, the Finite Element Method (FEM) has proven to be a versatile numerical tool applicable to chemistry, physics, and the biological sciences. Within the COMSOL Multiphysics environment, FEM can be effectively implemented across one, two, or three-dimensional domains, as illustrated by the following examples:

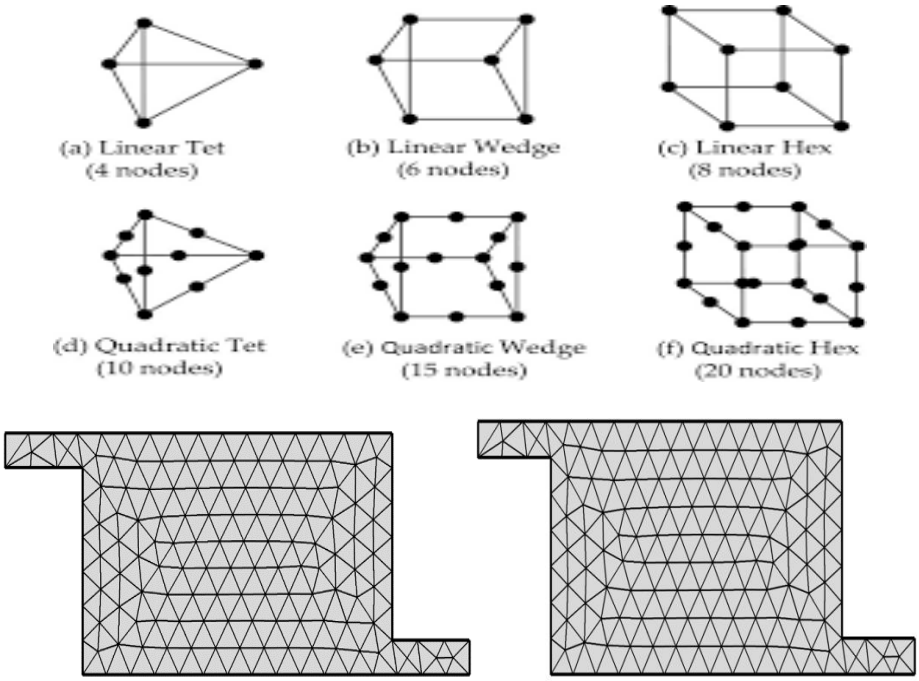

Figure – 2: various styles of the finite element discretization's

The different form elements, such as edges, nodes, and entire faces of the domain, are shown in Figure–2 above. After converting the derivatives into little unknowns with the necessary boundary value conditions, the set of discrete form equations was built using the individual node.

The FEM is a numerical technique that breaks down a complex domain into discrete, tiny components that may be calculated in relation to one another. The piecewise elements show the basic algebraic terms obtained from the discretization process of the FEM, and the entire domain describes the partial differential equations. Many CFD software, including ANSYS CFX, COMSOL Multiphysics, open Foam, and many more, use the FEM tool.

Numerous businesses and other physical and biological research sectors use the FEM tool. There are several uses for the material, including extensive use in the electrical, computer, and aerospace industries. These days, FEM is a very significant instrument in the biosciences and in the production of medications. In particular, it is necessary to model the structure of tissues and to simulate the flow of blood via arteries, bones, muscles, and many other structures. Additionally, FEM shown that modelling and simulation are superior to experimental methods.
Due of its widespread use in the literature, the FEM tool is used here. It is applied to the governing equations using the CFD application COMSOL Multiphysics. However, the

packages included several FEM systems like Petrov-Galerkin and Galer kin. To readily regulate the steady state solution of the governing equations, only Galer kin FEM was used in this case, along with the FEM and least squares procedure.

GALERKIN LEAST SQUARE FINITE ELEMENT TECHNIQUE

In the field of CFD, the Finite Element Method (FEM) is frequently employed to obtain numerical solutions for the Navier-Stokes equations, especially when dealing with complex partial differential equations. While other established techniques—such as the Lattice Boltzmann Method (LBM), the Finite Volume Method (FVM), and Boundary Element methods—are widely used across various CFD platforms and custom computational codes, this study utilizes individual FEM models tailored for elasticity, fluid mechanics, and structural mechanics. Specifically, a hybrid approach is implemented here to solve the governing PDEs by integrating the Least Squares stabilization technique with the traditional Finite Element framework. When it comes to handling with discrete circumstances, removing the attribute of symmetry, and dealing with positive definite simple systems, LSGFEM is a more dependable and driven methodology that covers all the advantages of Rayleigh-Ritz techniques. This approach is centered on optimizing convex unknowns that are created using system of equation residuals. In the context of solving partial differential equations, the Least-Squares Galer kin Finite Element Method (LSGFEM) is fundamentally characterized by forcing the functional residuals into an orthogonal direction relative to the finite element subspaces. Integrating the least-squares process into the finite element framework offers significant practical advantages, including the rapid development of bases for compatible subspaces, the efficient construction of linear systems, and the improved well-posed Ness of those systems. Furthermore, LSGFEM provides distinct benefits over traditional FEM or Rayleigh-Ritz methods; most notably, the least-squares residual functions as a reliable error indicator that can be directly used to drive adaptive mesh refinements. Consequently, this approach allows residuals from both homogeneous and non-homogeneous boundary conditions to be seamlessly integrated into the minimization of the least-squares unknowns. The Least-Squares Galer kin Finite Element Method (LSGFEM) serves as a robust approach for solving Navier-Stokes problems in fluid mechanics, offering a more dependable and computationally efficient means of resolving the unknowns within partial differential equations—particularly when applied to first-order systems. To leverage these advantages, the standard second-order Navier-Stokes equations are transformed into a vorticity-velocity-pressure formulation by introducing vorticity as an additional parameter.

PROCEDURE OF FIRST ORDER SYSTEM THROUGH LSGFEM

The numerical strategy implemented in this study is the Least-Squares Galer kin Finite Element Method (LSGFEM), which is strictly designed for first-order systems of equations. Because the governing momentum and continuity equations are initially second-order, an algebraic transformation is required to eliminate higher-order terms. To achieve this, vorticity—defined as the curl of the velocity field—is introduced as an auxiliary variable. This transformation allows the system to be recast into a more manageable first-order framework. The specific procedures for this conversion are described below:

$$\nabla . \boldsymbol{u} = 0 \tag{6}$$

$$-\frac{1}{\mathrm{Re}}\nabla^2 \boldsymbol{u} + \nabla P + \boldsymbol{u}(\nabla \boldsymbol{u}) = 0 \tag{7}$$

Now added extra parameter Vorticity that are:

$$\boldsymbol{w} = \nabla \times \boldsymbol{u} \tag{8}$$

As per identity of vector analysis, it is described as below;

$$\nabla \times (\nabla \times u) = -\nabla^2 .u \tag{9}$$

After the equations (8) and (9) substituted into the (7), the resulted the system described below;

$$\nabla . \boldsymbol{u} = 0 \tag{10a}$$

$$\boldsymbol{u}.\nabla \boldsymbol{u} + \frac{1}{\mathrm{Re}} \nabla \times \boldsymbol{w} + \nabla p = 0 \tag{10b}$$

$$w - \nabla \times \boldsymbol{u} = 0 \tag{10c}$$

The necessary problem is two-dimensional, the fluid is Newtonian and incompressible, and it may be expressed in the form of Cartesian coordinates as follows:

$$\frac{\partial \mathrm{u}^*}{\partial x^*} + \frac{\partial \mathrm{v}^*}{\partial y^*} = 0 \tag{11a}$$

$$u \frac{\partial u^*}{\partial x} + v \frac{\partial u^*}{\partial y} + \frac{\partial P}{\partial x} + \frac{1}{\mathrm{Re}} \frac{\partial w^*}{\partial y} = 0 \tag{11b}$$

$$u \frac{\partial \mathrm{v}^*}{\partial x} + v \frac{\partial \mathrm{v}^*}{\partial y} + \frac{\partial P}{\partial y} - \frac{1}{\mathrm{Re}} \frac{\partial \mathrm{v}^*}{\partial x} = 0 \tag{11c}$$

$$w^* + \frac{\partial u^*}{\partial y} - \frac{\partial v^*}{\partial x} = 0 \tag{11d}$$

The system (11) is now referred to as a first order system. The matrix system of all unknowns (u, v, P, and w) with regard to x and y may be used to further solve the problem.

.

$$\mathrm{A}_1 = \begin{pmatrix} 1 & 0 & 0 & 0 \\ u & 0 & 1 & 0 \\ 0 & u & 0 & -\frac{1}{\mathrm{Re}} \\ 0 & -1 & 0 & 0 \end{pmatrix}, \qquad \mathrm{A}_2 = \begin{pmatrix} 0 & 1 & 0 & 0 \\ v & 0 & 0 & \frac{1}{\mathrm{Re}} \\ 0 & v & 1 & 0 \\ 1 & 0 & 0 & 0 \end{pmatrix}$$

$$\mathrm{A} = \begin{pmatrix} 0 & 0 & 0 & 0 \\ 0 & 0 & 0 & 0 \\ 0 & 0 & 0 & 0 \\ 0 & 0 & 0 & 1 \end{pmatrix}, \qquad f = \begin{pmatrix} 0 \\ 0 \\ 0 \\ 0 \end{pmatrix}, \qquad \mathbf{u} = \begin{pmatrix} u \\ v \\ p \\ w \end{pmatrix}$$

The system KU = F is now discretized using the least square Galer kin FEM, and the stiffness matrix (k) is solely calculated using the subsequent procedure:

$$\mathrm{L}\Psi_j = \Psi_{j,x} \mathrm{A}_1 + \Psi_{j,y} \mathrm{A}_2 + \psi_j \Psi \tag{12a}$$

$$\mathrm{K}_e = \int_{\Pi_d} <\mathrm{L}\Psi_1, \mathrm{L}\Psi_2, \mathrm{L}\Psi_3, ..., \mathrm{L}\Psi_{Ne}>^{\mathrm{T}} <\mathrm{L}\Psi_1, \mathrm{L}\Psi_2, \mathrm{L}\Psi_3, ..., \mathrm{L}\Psi_{Ne}> \mathrm{d}\Pi \tag{12b}$$

Following the assembly of the global stiffness matrix K, the discrete algebraic system is formulated as KU = f to solve for the velocity field (u and v), pressure (p), and vorticity (ω).

To resolve this system efficiently, the Newton-Raphson method was selected as the most appropriate numerical instrument. This iterative methodology is particularly well-suited for these equations due to its superior convergence properties when handling the non-linearity inherent in fluid flow.

NEWTON RAPHSON METHOD

Primarily recognized as a robust iterative process, this method was famously detailed by reported literature [31] for resolving non-linear equations involving a single variable. While initially utilized across various physical disciplines for single-unknown problems, the evolution of computer algorithms has greatly extended its application to complex systems of both linear and non-linear equations with multiple variables. This approach has been widely integrated into modern CFD software, most notably COMSOL Multiphysics, which leverages the technique to efficiently manage non-linear research problems. By utilizing this method, the software maintains a controlled number of iterations while ensuring the solution reaches the required threshold of numerical accuracy.

$$x^*_{i+1} = x^*_i - \frac{f\left(x^*_i\right)}{f'\left(x^*_i\right)} \qquad i = 0, 1, 2, 3,.... \tag{13}$$

Equations (3–13) may be transformed into the Jacobean determinant form, which is as follows:

$$x^*_{i+1} = x^*_i - J\left(x^*_i\right)^{-1} f\left(x^*_i\right) \qquad i = 0, 1, 2, 3,.... \tag{14}$$

However, $J\left(x_i\right)^{-1}$ is sometimes referred to as the Jacobean matrix, which has the following definition and is recognized as the inverse matrix of all differentials of unknowns in terms of x and y;

$$J(x)^{-1} = \begin{bmatrix} \frac{\partial f_1}{\partial x_1}(x) & \frac{\partial f_1}{\partial x_2}(x)..... & \frac{\partial f_1}{\partial x_n}(x) \\ \frac{\partial f_2}{\partial x_1}(x) & \frac{\partial f_2}{\partial x_2}(x)..... & \frac{\partial f_2}{\partial x_n}(x) \\ . & . & ..... & . \\ . & . & ..... & . \\ . & . & ..... & . \\ \frac{\partial f_n}{\partial x_1}(x) & \frac{\partial f_n}{\partial x_2}(x)..... & \frac{\partial f_n}{\partial x_n}(x) \end{bmatrix}$$

To compute the unknowns from equations (14), it is necessary to establish an initial guess for all variables. In this study, these initial values—covering the velocity components, pressure, and vorticity—are assumed to be zero. By initializing the system at $U^{(0)} = 0$, the iterative process described above is applied to the governing equations to reach a converged solution.

RESULTS AND DISCUSSION

The power law concept, which stated that all fluids had constant viscosity, was followed by Newtonian fluids. Chemical engineers and chemical industries use these fluids through the

backward step duct extensively. For example, they are used to design water bottles, study how water fluids behave in these bottles, and analyse the patterns of molecular mixing in bioreactors. The backward step duct has a wide range of possible uses in major companies that are specifically constructed for water tanks and interpret the behavior of water via these tanks. As a result, backward step duct flows are specifically employed in the automotive industry to create silencers or mufflers for large automobiles.In order to create the greatest CFD packages, these mufflers were used in sports cars. They looked at air flows and managed the loud noises they produced [22-24].

The free surface shallow water flows across the rectangular basin domain that are connected to the forward and backward step ducts were studied [30]. Three methods—theoretical, finite volume tool using the CFD program WOLD 2D and experimental—were examined for the turbulence flow patterns. Different rectangular basin geometries with varying hydraulic conditions were discussed, including variations in the basin's width and length. It was discovered that these geometries either provided symmetric conditions for inflow or had non-symmetric flow patterns, and various Froude numbers were evaluated.According to the findings, symmetric vortices were detected in small basins, but as the basins' length and breadth increased, non-symmetric vortices were also seen. Three distinct types of vortices were discovered: lower, upper corner and main core flow vortices. Additionally, using the CFD software, the stable projected outcomes of the streamline flow characteristics were expressed.

By using experimental methods and WOLD 2D turbulence models, [25] were also able to mimic the geometry of shallow water reservoirs, such as backward and forward step channels. The Reynolds-AveragedNavier-Stokes equations for shallow seas were used to calculate the velocity profile using the k–Ɛ model with finite volume discretization technique. River engineering and urban hydraulics served as the foundation for this concept. In order to alter the ratio, a number of flow characteristics at various geometries, including average velocity profiles, velocity flow patterns, and turbulent energy, both kinetic and average kinetic, which were relevant for the global indicator were calculated.Every flow pattern was examined experimentally before being contrasted with the WOLF 2D package's predicted outcomes. It was determined that mean flow characteristics were more accurately and steadily measured using the k-turbulent model.

To investigate Newtonian flow phenomena across various expansion ratios of 1:4, 1:6, and 1:8 in converging and diverging channels, a finite volume model using the ANSYS Fluent CFD platform was developed as reported [26]. The study utilized the Gambit package to design and mesh specific geometries, including a basin and a backward-facing step channel with varying length-to-width ratios, before exporting them to the solver. These geometries were used to analyze laminar flow characteristics by coupling pressure and velocity within the Navier-Stokes equations, focusing on both clear-flow and porous-media configurations. By varying the Reynolds number, literature shows that laminar streamline patternswere demonstrated, calculated reattachment lengths, and determined recirculation flow rates. The results revealed the formation of distinct eddies in the primary core flow as well as in the upper and lower corners of the backward-facing step. As the Reynolds number increased, these vortices transitioned into non-symmetric patterns, illustrating the evolution of the vortex phenomenon.

PROBLEM SPECIFICATIONS WITH NECESSARY CONDITIONS

Selecting a rectangle domain with a fixed rectangular tiny channel as an upper inlet and another rectangular as an exit at the lower level is the challenge of interest. The schematic design defines the total dimensions for both the small and large channel segments, incorporating no-slip boundary conditions at all stationary walls to account for fluid friction.Because the governing equations are parabolic,fixed the parabolic velocity profile at inlet as $u = f(y) = 10 \times U_{max} \times y(1 - y)$ and imposed zero pressure at outlet of the channel.

Select triangle pieces for the domain's mesh design on both the boundaries and throughout the domain. The total number of triangle elements is thus 4704; there are 252 edge elements, 8 vertex elements, and 7437 degrees of freedom correspondingly. The element has a minimum size of $1.2\times10^{-3}$and a maximum size of 6×10^{-3}. The precision is highest at the smallest size. The high degree of correlation between the current results and the established data [27-29] validates the accuracy of the findings obtained through the GLSFEM approach.

DISCUSSIONS OF THE PREDICTED RESULTS

The discussion is predicated on the anticipated outcomes obtained by using the finite element method with Galer kin least square residuals included. The anticipated outcomes center on the examination of Newtonian and incompressible fluid transport through the different backward step duct ratios. The fluids were analysed based on the impacts of the ratio in the domain with a fixed Reynolds number and the various Reynolds numbers. The flow patterns were seen as velocity streamlines, and vortex measurements were seen at the domain's corners.

INFLUENCE OF THE REYNOLDS NUMBER ON FLOW PATTERNS OF THE DIFFERENT RATIOS IN THE BACKWARD STEP DUCT

The actual backward step duct domain was first designed with the required initial and boundary conditions at each zone of the duct, mesh structures, velocity streamlines, and flow feature plots such as vortex length and intensity as recirculation flow rate based on the Reynolds number. Figure 3 first outlined the study problem's schematic domain, which is referred to as a backward step channel with a tiny channel as the outlet. Due to the immovable walls, the domain has a parabolic intake, zero pressure at the exit, and Neumann boundary conditions. For both the 1:6 and 1:12 ratios of the backward step channel, Figure 4 described the finer, highly refined, and structured meshes in the continuity.

The triangular finite element structure with the smallest step size (1.3×10^{-3}) is selected. The streamline laminar flow patterns of the velocity and varying varied Re's were described in Figure 5(a). Surprisingly, the expansion channel's left quiet corner displays the relatively thin primary eddy. As Re increases, the size of the main eddy increases and moves toward the channel's exit, but no secondary eddy appears at lower Re values (= 300). The flow phenomena are also changed in figure 5(b). As a result of the higher Re's, the primary eddy is larger, more visible in the quiet corner of the expansion channel, and almost fills the whole space of the core flows.

Re=300 also starts the secondary vortex in the top corner of the expansion channel, and when Re increases to 700, the secondary eddy gradually enlarges in the upper right corner of the expansion channel. At the lower left corner of the backward step duct, another secondary vortex is also visible. The streamline patterns for the backward step channel's enlarged 1:12

ratio were shown in Figure 6(a and b). Here, the ratio was raised to 1:12 in order to expand the size of the channel's extension section. Both primary and secondary eddies, which are not generated in the lower ratio (1:6), are initially seen as a result of the ratio being enhanced (Re = 01).Additionally, when Re increases, the primary vortex's size increases significantly in both horizontal and vertical directions, while the secondary eddy's size gradually increases at the corners of the channel's expansion section. As a result, when Re's are increased, the primary eddy is clearly seen to be enhanced both vertically and horizontally at the left silent corner of the channel's expansion portion, but the secondary vortex's size enhancement at the upper right corner of the channel's expansion portion occurs far too slowly.

The enormous primary eddy is then readily visible at the expansion channel's quiet corner and fills the whole expansion part of the channel with the large eddy when Re's are increased to 500. Likewise, the top right corner of the channel's expansion section exhibits a fairly gradual increase in the size of the secondary eddy. The calculations are raised to the Reynolds number 1000 as a result of increasing the ratio from 1:6 to 1:12.Three distinct vortices are seen in the more streamline laminar flow patterns depicted in Figure 7: the major vortex at the bottom corner (main core flow), the secondary vortex at the upper right corner, and the tertiary vortex at the lower corner of the backward step duct. The calculations begin with Re = 700 and go up to 1000. The magnitude of the primary vortex in the main core flow is clearly visible, while the secondary and tertiary vortices are growing but moving extremely slowly and too slowly, respectively.

INFLUENCE OF THE ASPECT RATIOS ON FIXED REYNOLDS NUMBER

The effect of increasing the ratio from 1:6 to 1:12 in the channel's expansion portion with fixed Re = 01, 200, 300, and 600 is shown in Figure 8(a). At the lowest Reynolds number (=01), only the primary eddy is visible in the left corner of the channel, but at the large ratio (1:12), both primary and secondary tinny eddies are visible in each corner of the channel's expansion portion. As Reynolds number (200) is increased, the primary vortex increases in both ratios, but the size of the vortex is higher in the ratio 1:12 to 1:6. The secondary vortex grows in size, but it does so very slowly that it is insignificant.The streamline patterns with higher Reynolds numbers (300 to 600) were also shown in Figure 8(b). The tertiary vortex developed in the bottom corner of the backward step duct and expanded slowly, while the primary and secondary vortices were clearly visible and further increased. The enhancement of the Reynolds number is found to increase the vortex size in all streamline flow patterns; however, the enhancement is smaller in the low ratio (1:6), with the exception of the stronger enhancement in the higher ratio (1:12) of the backward step duct. Plotting the recirculation flow rate as a function of the rising Reynolds number so justifies improvement.

The similar enhancement was shown in Figure 9 as a result of an increase in Reynolds number. Both plots showed the enhancement, but they also showed the rapid linear enhancement in the recirculation flow rate for the larger ratio of 1:12 of the backward step duct. Additionally, Figure 9(a – d) depicted the plot of the primary vortex length calculations seen in the streamline laminar flow patterns, making it evident that the primary vortex increases gradually in the lower ratio (1:6) and quickly in the higher ratio (1:12) of the backward step duct. The detailed quantitative values of the vortex length and recirculation flow rate in size with varying Reynolds numbers were lastly given in tables 1 and 2.In this study, the empirical equations for both geometry ratios were freshly calculated using statistical measures as least square regression equations. The maximum value of the recirculation flow rate with different Reynolds numbers, which are mentioned below, is the main emphasis of these empirical formulae;

For ratio 1:6

$$X_{16} = 1.97723e-06\,\mathrm{Re} + 4.3645e-03 \qquad 1 \le \mathrm{Re} \le 600$$

For ratio 1:12

$$X_{12} = 1.98797e-06\,\mathrm{Re} + 4.487e-03 \qquad 1 \le \mathrm{Re} \le 1000$$

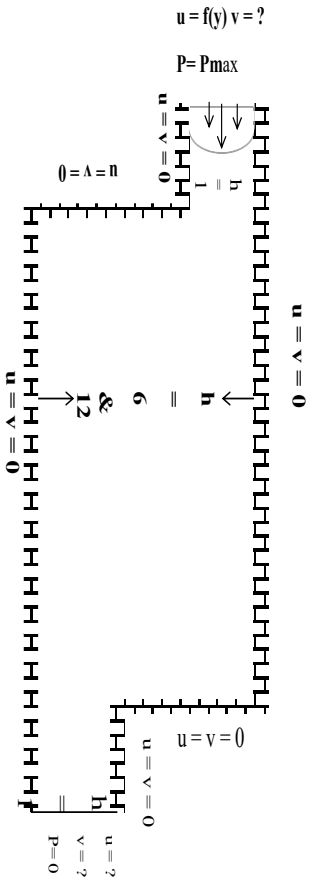

Figure–3: The two-dimensional rectangular backward step duct's schematic diagram.

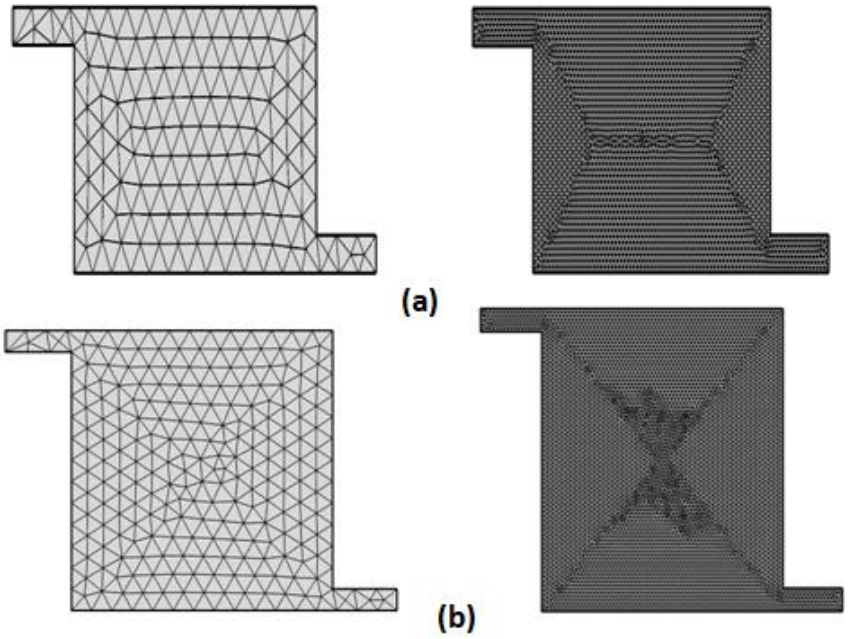

Figure–4: The rectangular backward step duct's finer and very small mesh for ratios (a) 1:6 and (b) 1:12.

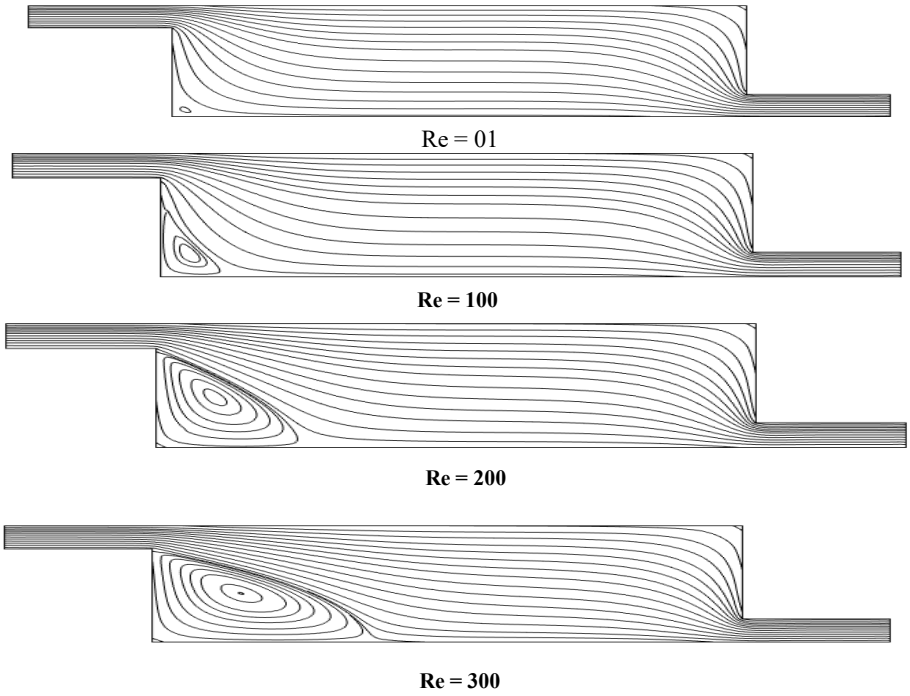

Figure –5(a): Simplify the 2-D backward step duct's velocity contours at a 1:6 ratio ($01 \leq Re \leq 300$).

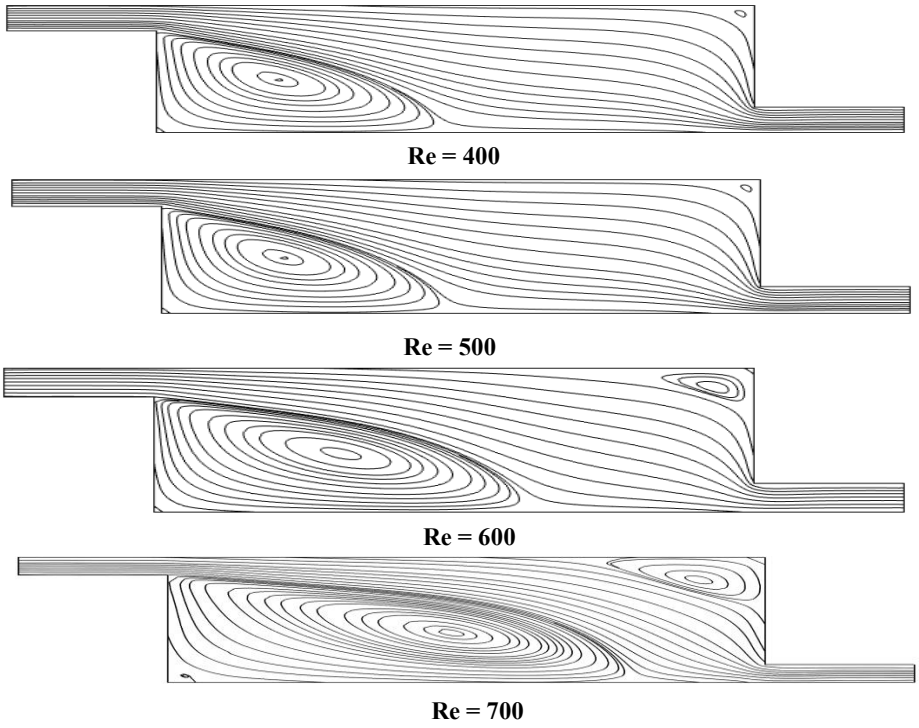

Figure –5(b): Simplify the 2–D backward step duct's velocity contours at a 1:6 ratio (400 ≤ Re ≤ 700).

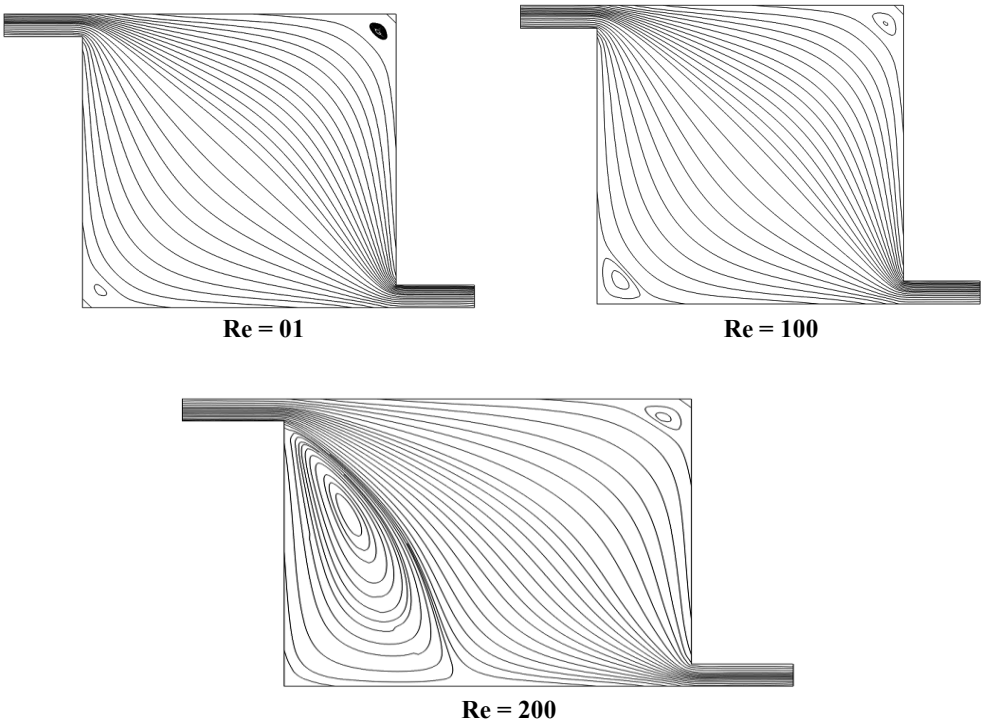

Figure –6(a): Simplify the 2–D backward step duct's velocity contours in a 1:12 ratio (01 ≤ Re ≤ 200).

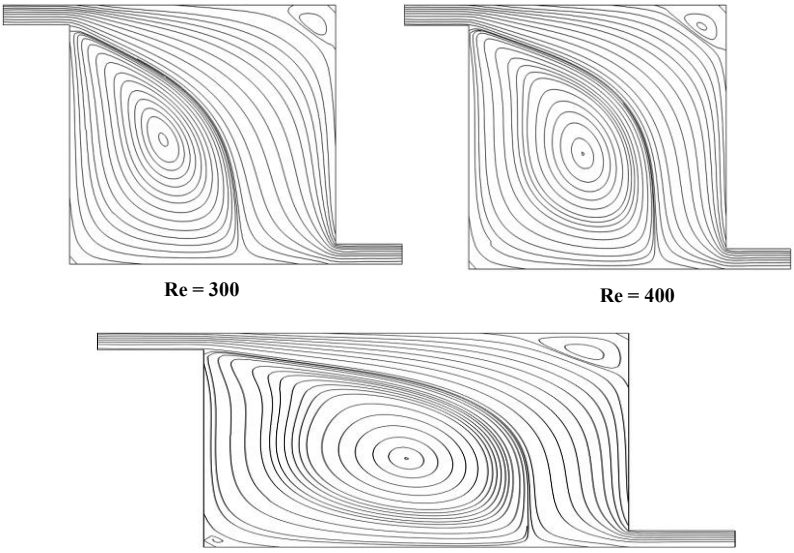

Figure –6(b): Simplified Velocity Contours of the 2–D Backward Step Duct at a 1:12 Ratio

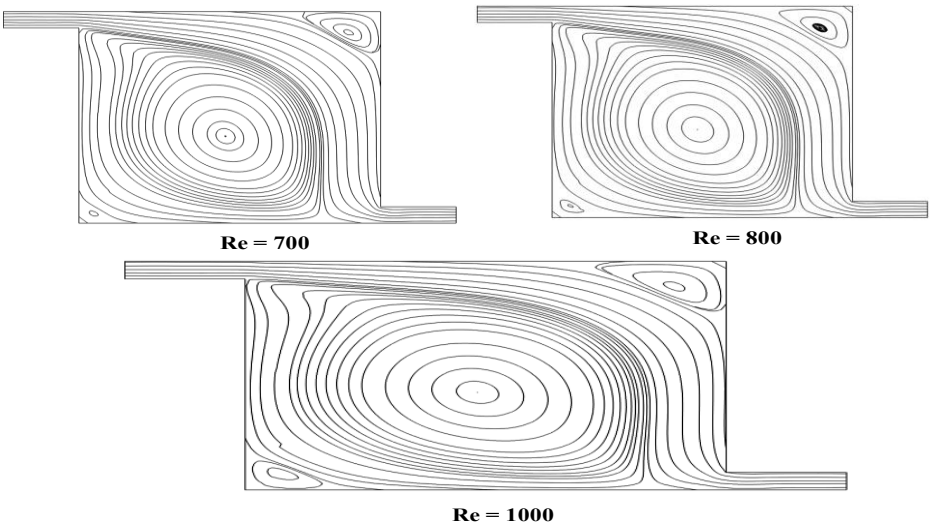

Figure –7: Simplify the 2–D backward step duct's velocity contours in a 1:12 ratio ($700 \leq Re \leq 1000$).

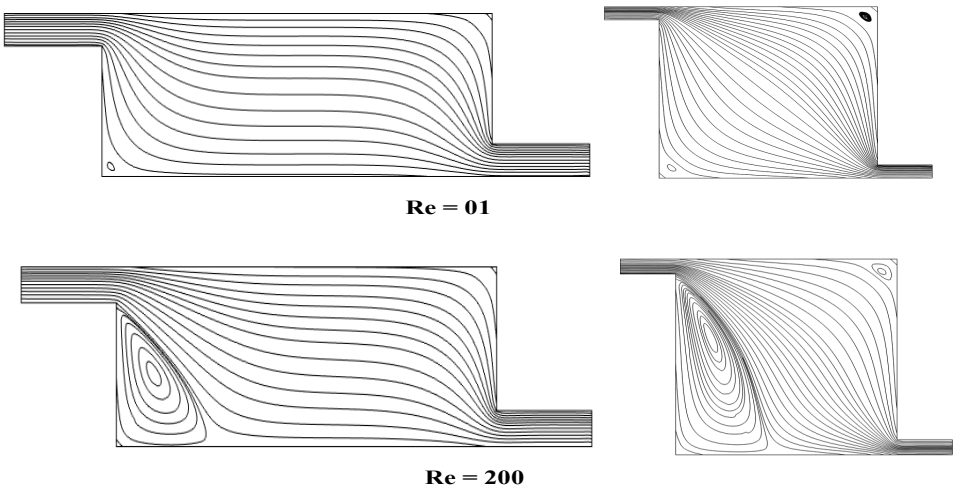

Figure –8(a): Using fixed Re = 01 and 200, streamline the velocity contours of the 2–D backward step duct in various ratios (1:6 and 1:12).

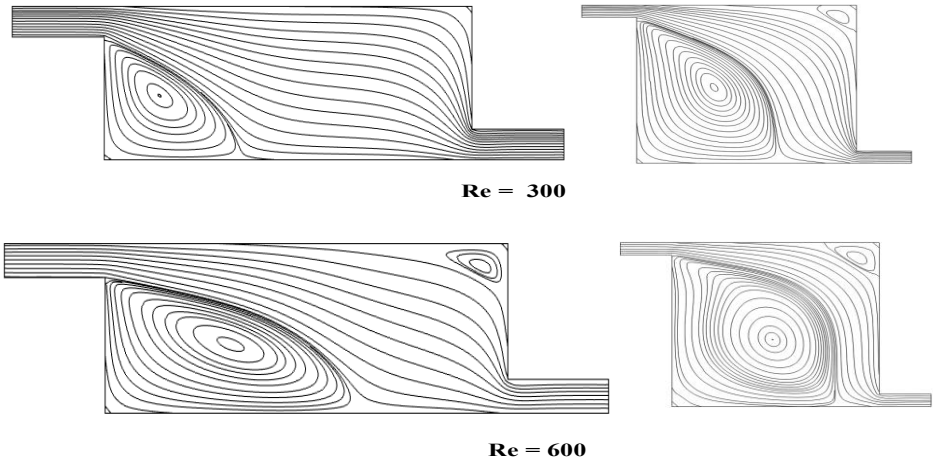

Figure –8(b): The 2–D backward step duct's streamline contours of velocity in various ratios (1:6 and 1:12) with fixed Re = 300 and 600.

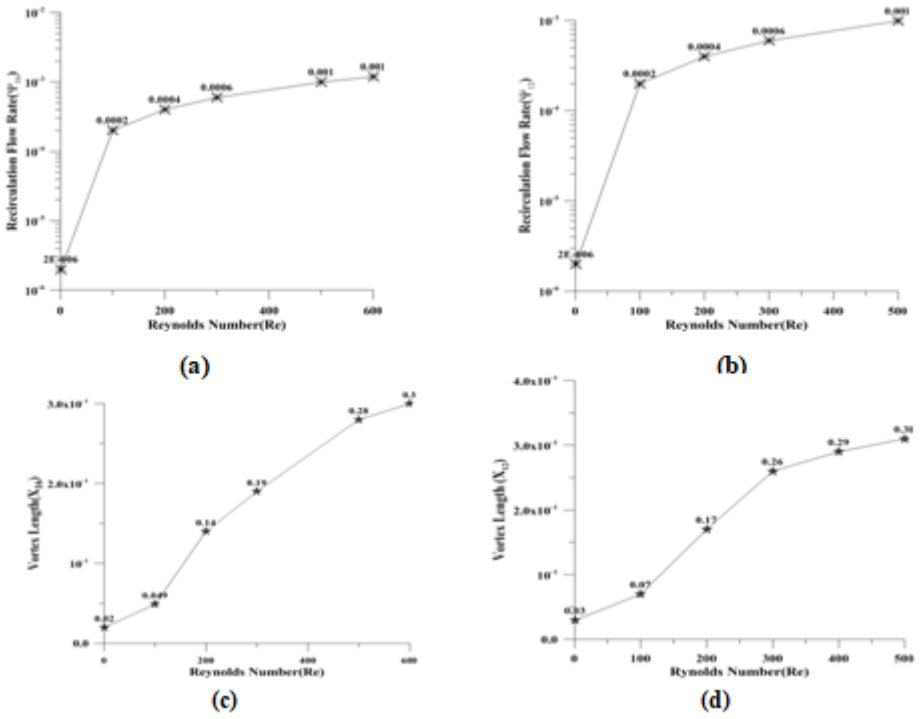

Figure –9(a, b, c, d): Vortex length (X) at different Reynolds numbers (Re) for the 2-D backward step duct in different ratios (1:6 and 1:12) and recirculation flow rate at different Reynolds numbers (Re).

Table–1: Recirculation flow rate minimum and maximum values at various Reynolds numbers for the 1:6 and 1:12 2-D backward step duct ratios

Recirculation Flow rate(Ψ)					
Reynolds number(Re)	**Ratio of the domain (1:6)**		**Reynolds number(Re)**	**Ratio of the domain (1 :12)**	
	($\Psi_{1\,min}$)	**($\Psi_{1\,max}$)**		**(Ψ_{2min})**	**(Ψ_{2max})**
600	1.03×10^{-8}	1.19×10^{-3}	500	4.47×10^{-10}	9.94×10^{-4}
500	1.83×10^{-10}	1.08×10^{-3}	400	1.99×10^{-10}	7.97×10^{-4}
400	3.54×10^{-9}	7.96×10^{-4}	300	5.87×10^{-11}	5.99×10^{-4}
300	6.81×10^{-9}	5.98×10^{-4}	200	8.23×10^{-11}	4.00×10^{-4}
200	2.57×10^{-10}	4.00×10^{-4}	100	2.74×10^{-11}	2.01×10^{-4}
100	7.81×10^{-11}	2.01×10^{-4}	50	1.28×10^{-11}	1.00×10^{-5}
50	5.25×10^{-11}	1.00×10^{-4}	1	2.47×10^{-13}	2.00×10^{-6}
1	1.14×10^{-12}	2.00×10^{-6}			

Table–2: Vortex Length (X) at various Reynolds Numbers for the 2–D backward step duct ratios of 1: 6 and 1:2.

Vortex Length(X)			
Reynolds number(Re)	**Ratio of the domain (1:6)**	**Reynolds number(Re)**	**Ratio of the domain (1 :12)**
	(X)		**(X)**
600	0.300	500	0.310
500	0.280	300	0.260
300	0.190	200	0.70
200	0.140	100	0.070
100	0.049	01	0.030
01	0.020	-----	------

CONCLUSION

The numerical investigation concludes that the Galer kin Least Square Finite Element Method (GLSFEM) within the COMSOL Multiphysics environment effectively characterizes the complex flow phenomena of Newtonian fluids in a backward step duct. The study successfully demonstrates that both fluid inertias, represented by the Reynolds number, and geometric variations, specifically aspect ratios of 1:6 and 1:12, significantly influence vortex formation and flow stability. Results indicate that increasing the Reynolds number and expansion ratio leads to enhanced intensity and length of primary, secondary, and even tertiary eddies at the duct corners. Quantitative findings, supported by newly developed empirical equations for recirculation flow rates, reveal a quick linear enhancement in the higher aspect ratio of 1:12 compared to the 1:6 ratio. Ultimately, these insights into flow separation and reattachment provide essential predictive tools for optimizing industrial designs in fields such as automotive engineering, aerospace, and chemical processing to improve flow control and energy efficiency.

Author Contribution

Murtaza Hussain Shar conceptualized, designed experiments, Dr. Abdul Raheem Shar prepared the draft of the article Mazhar Ali Sahito and Akhalque Ahmed Abbasi interpreted the data. All authors read, revised, and approved the final version of the manuscript.

Acknowledgements

The authors acknowledge the facilities provided by the Department of Mathematics, Shah Abdul Latif University Khairpur and also technical support provided by department of Statistics, Shah Abdul Latif University Khairpur.

Conflict of Interest

The authors declare no conflict of interest

References

1. Tu, J., Yeoh, G.H., Liu, C. and Tao, Y., 2023. *Computational fluid dynamics: a practical approach*. Elsevier.
2. Patil, D. and Kadam, S., 2023, January. Basics of computational fluid dynamics: An overview. In *IOP conference series: Earth and environmental science* (Vol. 1130, No. 1, p. 012042). IOP Publishing.
3. Zhou, L., Elemam, M.A., Agarwal, R.K. and Shi, W., 2024. Computational fluid dynamic (CFD). In *Discrete Element Method for Multiphase Flows with Biogenic Particles: Agriculture Applications* (pp. 65-82). Cham: Springer Nature Switzerland.
4. Sahito, M.A., Abbasi, A.A., Shar, M.H. and Rid, R.A., 2026. MATHEMATICAL MODELLING OF NEWTONIAN FLUIDS FLOW PHENOMENA THROUGH DIFFERENT RATIOS OF BACKWARD STEP DUCT. *Kashf Journal of Multidisciplinary Research*, *3*(01), pp.65-104.
5. Taha, H., Gonzalez, C. and Shorbagy, M., 2023. A minimization principle for incompressible fluid mechanics. *Physics of Fluids*, *35*(12).
6. Wang, S., 2022. Extensions to the Navier–Stokes equations. *Physics of Fluids*, *34*(5).
7. Djojodihardjo, H., 2023. Conservation Principles in Fluid Mechanics and Potential Flow Aerodynamics. In *Introduction to Aeroelasticity: With Case-Studies* (pp. 113-189). Singapore: Springer Nature Singapore.
8. Ost, A.P., 2022. Analysis of stationary and non-stationary phenomena in turbulent subcritical flow behind two parallel cylinders.
9. Huang, C., Borthwick, A.G. and Lin, Z., 2022. Lagrangian coherent structures in flow past a backward-facing step. *Journal of Fluid Mechanics*, *947*, p.A4.
10. Ju, X. and Jiang, H., 2022. Secondary vortex street in the wake of a rectangular cylinder: Effects of Reynolds number, aspect ratio and free-stream perturbation. *International Journal of Heat and Fluid Flow*, *93*, p.108893.
11. Yadav, S. and Ganesan, S., 2023. *Data Driven Stabilization Schemes for Singularly Perturbed Differential Equations* (Doctoral dissertation, PhD thesis, Indian Institute of Science Bangalore–560 012 (India).
12. Cengizci, S., 2024. A SUPS formulation for simulating unsteady natural/mixed heat convection phenomena in square cavities under intense magnetic forces. *The European Physical Journal Plus*, *139*(8), p.713.
13. Zhang, Y., Xiao, Q., Zhang, G., Huang, H. and Zhang, Z., 2025. Evaluation of radial basis function selection and parameter optimization in cell-based smoothed radial point interpolation method for underwater acoustic prediction. *Engineering Analysis with Boundary Elements*, *180*, p.106499.
14. Idoko, I.P., Ezeamii, G.C., Idogho, C., Peter, E., Obot, U.S. and Iguoba, V.A., 2024. Mathematical modeling and simulations using software like MATLAB, COMSOL and Python. *Magna Sci. Adv. Res. Rev*, *12*, pp.62-95.
15. Beepat, K.G., Sharma, D.P., Pathak, D. and Mahajan, A., 2023. COMSOL Multiphysics-based modeling approach to solar cell development. *International Journal of Modern Physics B*, *37*(12), p.2350114.
16. Kenzhebekov, D.M., Khussanov, A.E., Iristaev, I., Zholshybek, A. and Janabayev, D., 2025. GENERATION AND CONFIGURATIONOF A HEAT EXCHANGER MODEL GRID FOR CFD MODELING IN COMSOL MULTIPHYSICS. *Механика және технологиялар*, (1 (87)), pp.279-285.
17. Rahman, M.S., 2024. Computational fluid dynamics for predicting and controlling fluid flow in industrial equipment. *European Journal of Advances in Engineering and Technology*, *11*(9), pp.1-9.

18. Naqash, T.M. and Alam, M.M., 2025. A state-of-the-art review of wind turbine blades: principles, flow-induced vibrations, failure, maintenance, and vibration suppression techniques. *Energies*, *18*(13), p.3319.
19. Memon, M.A., Ting, H., Cheah, J.H., Thurasamy, R., Chuah, F. and Cham, T.H., 2020. Journal of applied structural equation modeling. *Journal of Applied Structural Equation Modeling*.
20. Trivedi, R., Dai, H., Wang, Y. and Song, L., 2017, July. Know-evolve: Deep temporal reasoning for dynamic knowledge graphs. In *international conference on machine learning* (pp. 3462-3471). PMLR.
21. Budrienė, D. and Zalieckaitė, L., 2012. Cloud computing application in small and medium-sized enterprises. *Issues of Business & Law*, *4*.
22. Dewals, B.J., Kantoush, S.A., Erpicum, S., Pirotton, M. and Schleiss, A.J., 2008. Experimental and numerical analysis of flow instabilities in rectangular shallow basins. *Environmental fluid mechanics*, *8*(1), pp.31-54.
23. Herrera-Granados, O., 2021. Numerical analysis of flow behavior in a rectangular channel with submerged weirs. *Water*, *13*(10), p.1396.
24. Zhang, Y.Y., Lv, J.N., Yao, Z.D., Wang, Q. and Yan, X.F., 2025. Flow pattern adjustment subjected to effects of aquatic vegetation in a rectangular shallow basin from a numerical perspective. *Physics of Fluids*, *37*(4).
25. Camnasio, E., Erpicum, S., Archambeau, P., Pirotton, M. and Dewals, B., 2014. Prediction of mean and turbulent kinetic energy in rectangular shallow reservoirs. *Engineering Applications of Computational Fluid Mechanics*, *8*(4), pp.586-597.
26. Dufresne, M., Dewals, B.J., Erpicum, S., Archambeau, P. and Pirotton, M., 2011. Numerical investigation of flow patterns in rectangular shallow reservoirs. *Engineering Applications of Computational Fluid Mechanics*, *5*(2), pp.247-258.
27. Khajezade Roodi, M., Jalali, A., Hedayati, A. and Amiri Delouei, A., 2023. Optimization of Spark Ignition Engine Performance using a New Double Intake Manifold: Experimental and Numerical Analysis. *Journal of Applied and Computational Mechanics*, *9*(1), pp.1-14.
28. Ren, J.T., Wu, X.F. and Zhang, T., 2021. A 3-D numerical simulation of the characteristics of open channel flows with submerged rigid vegetation. *Journal of Hydrodynamics*, *33*(4), pp.833-843.
29. Souri, J., OmidvarMohammadi, H., Neyshabouri, S.A.A.S., Chooplou, C.A., Kahrizi, E. and Akbari, H., 2024. Numerical simulation of aeration impact on the performance of a-type rectangular and trapezoidal piano key weirs. *Modeling Earth Systems and Environment*, *10*(4), pp.5205-5224.
30. Yu, M., Modesti, D. and Pirozzoli, S., 2023. Direct numerical simulation of flow in open rectangular ducts. *Journal of Fluid Mechanics*, *977*, p.A32.
31. Burden, R.L. and Faires, J.D., 2005. Numerical analysis 8th ed. *Thomson Brooks/Cole*.